physica status solidi

pss

www.pss-journals.com

reprint

WILEY-VCH

Phys. Status Solidi RRL **10**, No. 2, 153–157 (2016) / **DOI** 10.1002/pssr.201510386

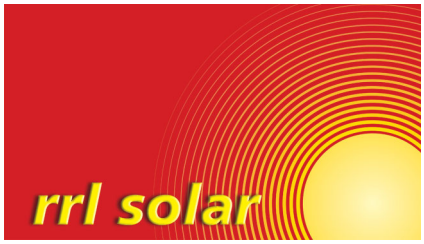

Low cost, high throughput and centimeter-scale fabrication of efficient hybrid perovskite solar cells by closed space vapor transport

Guijun Li*, Jacob Y. L. Ho, Man Wong, and Hoi-Sing Kwok

State Key Laboratory on Advanced Displays and Optoelectronics Technologies, Hong Kong University of Science and Technology, Clear Water Bay, Kowloon, Hong Kong

Received 21 October 2015, revised 14 November 2015, accepted 16 November 2015
Published online 20 November 2015

Keywords hybrid perovskites, solar cells, closed space vapor transport

* Corresponding author: e-mail gliad@connect.ust.hk

Hybrid perovskite solar cell is a fast-growing photovoltaic technology. Here, we present a method based on the closed space vapor transport deposition, which has the potential for large-scale production due to its low cost, high throughput, and large-area uniformity. We demonstrate $CH_3NH_3PbI_3$ solar cells with high power conversion efficiencies of 16.2%. Furthermore, the large area devices have high efficiency of 13.8% and good uniformity in a large substrate of 3 cm × 3 cm.

1 Introduction Over the past few years, one of the fastest growing areas of photovoltaic research that has sprung to the forefront of the scientific community involves a material called hybrid halide perovskites. The power conversion efficiency of solar cells using these hybrid perovskite compounds as the absorbing layer leaped from 3.8% as a forerunner in 2009 to a certified 20.1% in current versions [1, 2], rivalling most of the leading thin film solar cell technologies. The rapid pace of growth in perovskite solar cells has been attributed to a set of essential characteristics such as their strong light absorption, long-range balanced carrier transport length, exceptional defect tolerance and facile processability at low temperature [3–6].

Because of a very strong tendency to form and crystallize, even at room temperature, a hybrid perovskite can be conveniently deposited by a low temperature solution process, using a solution of two precursors, e.g., PbI_2 and CH_3NH_3I in the case of $CH_3NH_3PbI_3$. In a typical process, crystallization of perovskite occurs due to the evaporation of the organic solvent, where sometimes a low temperature annealing or a solvent extraction approach is subsequently employed to facilitate the solvent evaporation [7]. Besides the facile solution process, the vapor phase reactive process represents another important technique for the fabrication of hybrid perovskites. Typically, the organic halide and metal halide can react in the vapor state to form the perovskite compound. Co-evaporation of the organic halide and metal halide in a dual source vacuum chamber was conventionally applied and got much success in making efficient planar structure solar cells [8]. When the metal halide is in a solid-state, a two-step vapor phase process is widely used. The two-step vapor phase process is quite similar with the sequential solution process [9], in which the metal halide thin film is deposited on the substrate immediately following the reaction with the organic halide vapor. In some sense, the previously reported vapor-assisted solution process (VASP) [10], low pressure chemical vapor deposition (LPCVD) [11, 12], hybrid chemical vapor deposition (HCVD) [13], vapor-equilibrated regrowth (VERG) [14] or in situ tubular chemical vapor deposition (ITCVD) [15] can be considered for use as the two-step vapor phase process. These vapor phase processes enable better control of the film thickness and morphology, and can be applied to metal halides with poor solubility. However, most of them are predominantly based on lab

scale techniques, and tend to be, either in part or in full, time-consuming, energy-intensive and impractical in mass production. Translating these lab-scale processes to a large-scale production process is thus a pressing need for this promising photovoltaic technology.

Here, we report on a perovskite fabrication method that has the potential for large-scale production by closed space vapor transport (CSVT). CSVT is a scalable, low-cost and high-throughput technique for making semiconductors [16–18]. It is already a well-established industrial technology for cost-competitive, commercial-scale manufacturing of polycrystalline CdTe solar cells, along with explored device efficiencies of 19.6% [19]. With the CSVT process, we are able to make efficient perovskite solar cells with power conversion efficiencies of 16.2%. Moreover, this technique also takes advantages of the relatively inexpensive and compact design, high throughput, efficient precursor transport/utilization and good large-area uniformity. These features are significant because in order to successfully utilize perovskites for photovoltaic applications, the process must to be manufactured on a large-area substrate and at low-cost.

2 Results and discussion CSVT designed for the fabrication of the perovskite materials is illustrated in Fig. 1(a) with the deposition process detailed in the Experimental section (Supporting Information). In comparison to previously reported vapor phase processes such as the co-evaporation, VASP, and ITCVD, the high throughput is the key merits of the CSVT process, and relies on the following aspects: closed space, low pressure, and differential temperature. For example, in a vacuum based vapor process, the vapor has to transport over a long distance from the source (target) to the substrate, which will reduce the deposition rate and results in a lot of waste of the source material during the deposition. To increase the deposition rate the distance between the source and substrate must be shortened. A space smaller than the molecular mean free path also helps to satisfy the requirement of no molecular collision during the vapor transport [20], which makes the high vacuum unnecessary. On the other hand, comparing this to the VASP process which is conducted in atmosphere pressure [10], lowering the pressure favours the vapor transport and thus can largely reduce the process time, as shown in Fig. 1(b). At a chamber pressure of 50 mbar, it requires 10 min to fully convert the metal halide into the perovskite, whereas at a pressure of 1 mbar, 1.5 min is sufficient to totally transform the metal halide to the perovskite. Figure 1(c) shows an example of the $CH_3NH_3PbI_3$ film by placing the PbI_2 film into the CH_3NH_3I vapor. The obtained $CH_3NH_3PbI_3$ in Fig. 1(c) also shows good large-area uniformity in a size of 5 cm × 5 cm.

Similar to the other vapor phase process, the CSVT process can also be applicable to a wide range of material systems. Figure S1 in the Supporting Information (named SI in the following) illustrates the SEM images of

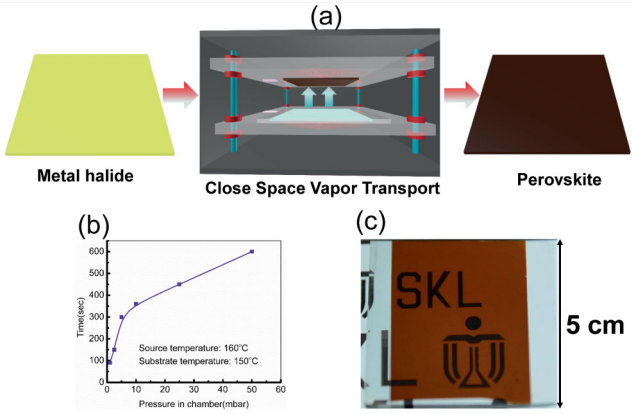

Figure 1 (a) Schematic illustration of closed space vapor transport deposition of hybrid perovskites; (b) process time required for the full transformation of PbI_2 into $CH_3NH_3PbI_3$ at different chamber pressures, the full transformation is identified by the colour change and the XRD spectra; (c) photograph of the $CH_3NH_3PbI_3$ film, with a size of 5 cm × 5 cm.

different perovskites produced from different metal halides ($PbCl_2$, PbI_2 and $PbBr_2$) and organic salts (CH_3NH_3I, CH_3NH_3Br). In these SEM images, $CH_3NH_3PbI_3$, $CH_3NH_3PbI_{3-x}Cl_x$ and $CH_3NH_3PbI_{3-x}Br_x$ are fabricated from close space sublimation of CH_3NH_3I, whereas $CH_3NH_3PbBr_3$, $CH_3NH_3PbBr_{3-x}I_x$ and $CH_3NH_3PbBr_{3-x}Cl_x$ are fabricated from close space sublimation of CH_3NH_3Br. All of these vapor processed perovskite films exhibit a grain size from hundreds nanometers to micrometers and the grain-to-grain are densely interconnected with 100% full surface coverage.

It is widely reported that precursors have a huge impact on the resulting perovskite morphology in the solution process [21–23], especially in the case of Cl. Carefully analysing the SEM images in Fig. S1 shows that there is a little difference in the grain size and its distributions. For example, in the Cl based perovskites, the grain size is larger than the other perovskites, which is consistent with the observation in the solution process. However, the difference of the film morphology in the CSVT process is not obvious as in the solution process. A possible explanation is that during the crystallization, there exists a large amount of the organic halide vapor and therefore it is the organic halide, instead of the metal halide, determines the film morphology. Furthermore, the crystallization is processed at a relatively high temperature of 150 °C. Under the organic halide vapor, if a metal halide with different halide element is used, for example, in the reaction of $PbCl_2$ and CH_3NH_3I, the halide element Cl in the metal halide will mostly release from the film during the crystallization due to the low sublimation temperature of CH_3NH_3CI [24].

Figure 2 shows the X-ray diffractions (XRDs) of different perovskites fabricated from the CSVT process. Under the same organic halide vapor, the as-obtained perovskite films have almost the same diffraction peak po-

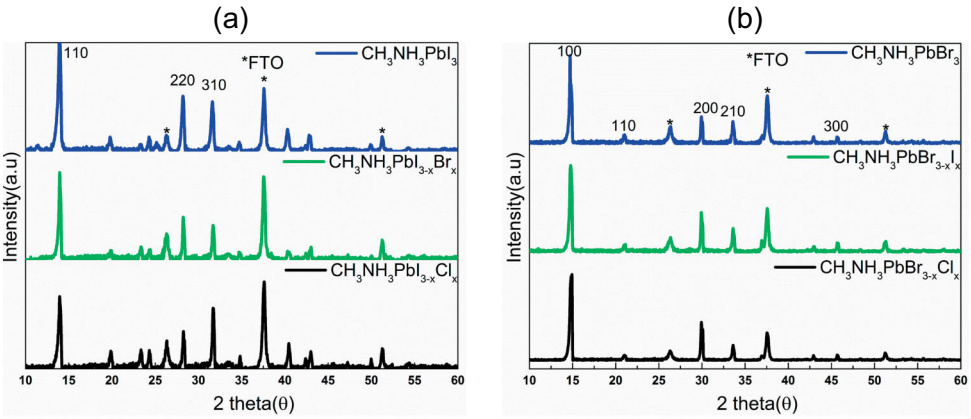

Figure 2 XRD spectra of perovskites obtained from closed space sublimation of (a) CH_3NH_3I vapor and (b) CH_3NH_3Br vapor.

sitions, no matter what the metal halide is. For example, as shown in Fig. 2(a), the main diffraction peaks at 13.95°, 28.26° and 31.72°, which are assigned to (110), (220) and (310), respectively, are in identical positions for $CH_3NH_3PbI_3$, $CH_3NH_3PbI_{3-x}Cl_x$ and $CH_3NH_3PbI_{3-x}Br_x$. The situation is also true for $CH_3NH_3PbBr_3$, $CH_3NH_3PbBr_{3-x}I_x$ and $CH_3NH_3PbBr_{3-x}Cl_x$, as shown in Fig. 2(b), which demonstrate their main crystal peaks (100), (110), (200), (210) and (300). However, there is still some difference in the peak intensity, especially the relative intensity for different diffraction peaks. This indicates the different growth orientations when different metal halides are used.

Optical properties such as the absorbance and complex refractive index are measured. Figure 3(a) shows the absorbance of perovskite films calculated from the ultraviolet–visible (UV–VIS) transmittance spectra. The as-obtained perovskite films have almost the same absorption behaviour under the same organic halide vapor, along with good consistency of the sharp band edge. Again, it seems that the type of the organic halide dominates the absorption behavior of the as-crystallized perovskite film in the CSVT process. By extrapolating the distinct linear region of the absorption edge to the abscissa in the Tauc plot (Fig. S2, SI), the optical bandgap of CH_3NH_3I group perovskites ($CH_3NH_3PbI_3$, $CH_3NH_3PbI_{3-x}Cl_x$ and $CH_3NH_3PbI_{3-x}Br_x$) and CH_3NH_3Br group perovskites ($CH_3NH_3PbBr_3$, $CH_3NH_3PbBr_{3-x}I_x$ and $CH_3NH_3PbBr_{3-x}Cl_x$) are determined to be 1.59 eV and 2.29 eV, respectively. The complex refractive index of $CH_3NH_3PbI_3$ obtained by variable-angle

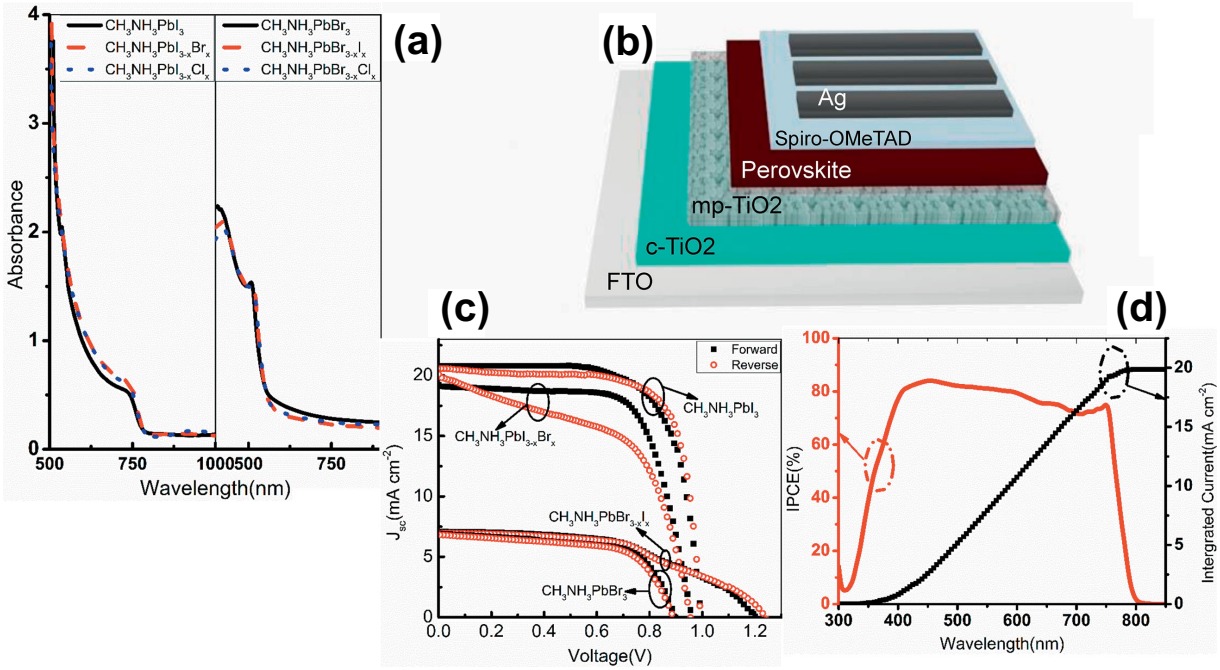

Figure 3 (a) Absorbance of CH_3NH_3I group perovskites ($CH_3NH_3PbI_3$, $CH_3NH_3PbI_{3-x}Cl_x$ and $CH_3NH_3PbI_{3-x}Br_x$) and CH_3NH_3Br group perovskites ($CH_3NH_3PbBr_3$, $CH_3NH_3PbBr_{3-x}I_x$ and $CH_3NH_3PbBr_{3-x}Cl_x$); (b) device architecture of perovskite solar cells used in this study; (c) typical *J–V* curves of $CH_3NH_3PbI_3$, $CH_3NH_3PbI_{3-x}Br_x$, $CH_3NH_3PbBr_3$, and $CH_3NH_3PbBr_{3-x}I_x$ cells under forward and reverse scan directions; (d) IPCE spectrum of the $CH_3NH_3PbI_3$ solar cell.

Table 1 Photovoltaic performance of perovskites solar cells. The forward and reverse scans are given. The average value is obtained from 8 cells for each.

perovskite	scan direction	V_{oc} (V)	J_{sc} (mA/cm^2)	FF (%)	PEC (%)
$CH_3NH_3PbI_3$	forward	0.99 ± 0.02	20.7 ± 0.3	72 ± 1	14.5 ± 0.7
	reverse	0.998 ± 0.03	20.4 ± 0.2	73.5 ± 0.5	15 ± 0.3
$CH_3NH_3PbI_{3-x}Br_x$	forward	0.954 ± 0.04	19.9 ± 0.6	55 ± 0.4	10.4 ± 0.3
	reverse	0.96 ± 0.03	19.2 ± 0.2	70 ± 1	12.9 ± 0.4
$CH_3NH_3PbBr_3$	forward	0.89 ± 0.03	6.9 ± 0.4	64 ± 2	4 ± 0.4
	reverse	0.9 ± 0.04	6.8 ± 0.5	63 ± 1.5	3.8 ± 0.6
$CH_3NH_3PbBr_{3-x}I_x$	forward	1.237 ± 0.05	7 ± 0.4	50 ± 3	4.3 ± 0.8
	reverse	1.240 ± 0.05	7 ± 0.4	53 ± 3	4.6 ± 0.7

spectroscopic ellipsometry (VASE) is also given in Fig. S3 (SI). The extinction coefficient exhibits three distinct peaks at 760 nm, 480 nm and 390 nm, which are consistent with that of the previously reported solution processed perovskites [25, 26].

Figure 3(b) illustrates a schematic diagram of the cell architecture with the perovskite absorbing layer deposited by the CSVT process. The cell performance can be influenced by the thermodynamic process of the sublimation, interdiffusion and crystallization in the CSVT process. After optimizing the source and substrate temperature (Fig. S4, SI), four types of perovskite solar cells are fabricated, with the photovoltaic characteristics shown in Table 1. The $CH_3NH_3PbI_3$ $CH_3NH_3PbI_{3-x}Br_x$, $CH_3NH_3PbBr_3$ and $CH_3NH_3PbBr_{3-x}I_x$ cells show average power conversion efficiencies of 15%, 12.9%, 3.8% and 4.6% in reverse scan. In the case of $CH_3NH_3PbBr_3$ and $CH_3NH_3PbBr_{3-x}I_x$ cells, surprisingly, there is a large difference in the V_{oc}. Higher V_{oc} is obtained for the $CH_3NH_3PbBr_{3-x}I_x$ cell which using the PbI_2 as the metal halide in the CSVT process of CH_3NH_3Br. However, in the case of $CH_3NH_3PbI_3$ and $CH_3NH_3PbI_{3-x}Br_x$ cells, the $CH_3NH_3PbI_3$ cell shows better performance than that of the $CH_3NH_3PbI_{3-x}Br_x$ cell. Figure 3(c) shows the forward and reverse scanned current–voltage curves of the typical perovskite solar cells. There is apparent hysteretic current–voltage behaviour in the $CH_3NH_3PbI_3$ and $CH_3NH_3PbI_{3-x}Br_x$ cells. However, the forward and reverse I–V curves are consistent in $CH_3NH_3PbBr_3$ and $CH_3NH_3PbBr_{3-x}I_x$ cells, indicating no hysteretic behaviour in these cells. The halide related hysteresis can be further studied in the future.

As an example, the current density of the $CH_3NH_3PbI_3$ cell under the applied bias voltage (0.837 V) at the maximum power point with a light soaking time is also provided (see Fig. S5, SI). A constant power conversion efficiency under continuous light illumination of 1 sun is observed. The corresponding IPCE of the $CH_3NH_3PbI_3$ cell is given in Fig. 3(d); the integrated J_{sc} from the IPCE curve is 19.9 mA/cm^2, which is in good agreement with that from the I–V measurement.

Cell area is important for large-scale development of perovskite solar cells. The above reported device area is 0.1 cm^2, which is also the most used area reported thus far in perovskite solar cells. Here we scale it up and down to investigate the potential large-scale fabrication of perovskite by the CSVT process for the $CH_3NH_3PbI_3$ cell. As shown in Fig. 4(a), cells of 0.01 cm^2 have the highest PCEs, with an average PCE of 15.7% and a champion PCE of 16.2%. The current–voltage and power–voltage curves

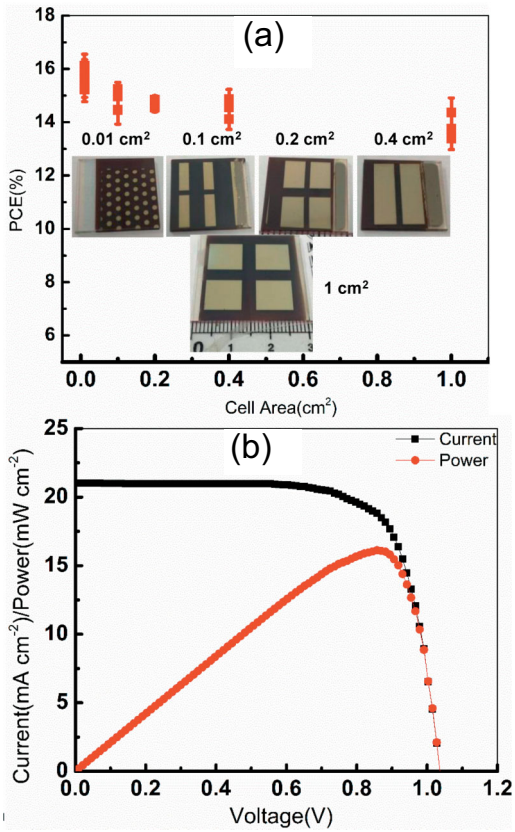

Figure 4 (a) Power conversion efficiencies of $CH_3NH_3PbI_3$ solar cells with different cell areas. The diameter of 0.01 cm^2 cell is 1.13 mm, the length × width in the 0.1 cm^2 cell is 0.5 cm × 0.2 cm, in the 0.2 cm^2 cell is 0.5 cm × 0.4 cm, in the 0.4 cm^2 cell is 1 cm × 0.4 cm, and in the 1 cm^2 cell is 1 cm × 1 cm. (b) C–V and P–V curves of the best $CH_3NH_3PbI_3$ cell.

of the champion cell are given in Fig. 4(b). When expanding the area to 0.2 cm^2, 0.4 cm^2 and 1 cm^2, the PCEs drop slightly down to 14.7%, 14.5% and 13.8 % respectively, whereas cells of 0.1 cm^2 shows an average PCE of 15%. Beside the area effect, the uniformity of the device is also essential to scale perovskite solar cells to large-area manufacturing. Figure S6 in the SI shows the distribution of the PCEs in a substrate of 3 cm × 3 cm from one typical process for the perovskite solar cells with 0.1 cm^2, 0.4 cm^2 and 1 cm^2 (the detailed V_{oc}, J_{sc}, FF and *XY* positions are given in supporting information). The substrate is divided into four sub-areas, with each sub-area containing 4 cells (of 0.1 cm^2 each), 2 cells (of 0.4 cm^2 each) and 1 cell (of 1 cm^2 each). As can be seen, only a negligible deviation of ±1% is found. It should be noted that the size of the homemade CSVT setup is 6 cm × 6 cm, the good uniformity achieved in a size of 3 cm × 3 cm with different cell areas indicates the potential of the CSVT process for large-scale fabrication.

3 Conclusion In summary, we have demonstrated that the CSVT is an efficient way to scale up the production of hybrid perovskite solar cells, mainly due to its simple design, and efficient precursor transport/utilization and good large-area uniformity. With the CSVT process, we find that perovskite compounds fabricated from the same organic halide have the same crystal structures and optical properties, no matter what the metal halide is. We show that the perovskites fabricated from the CSVT process have large grain size, pinhole free and good uniformity. We achieve high power conversion efficiencies of 16.2% for $CH_3NH_3PbI_3$ solar cells. Furthermore, the large area devices have high efficiency of 13.8% and good uniformity in a substrate of 3 cm × 3 cm, indicating the potential of the CSVT process for manufacturing low cost, high throughput and large-area efficient perovskite solar cells in the future.

Supporting Information Additional supporting information may be found in the online version of this article at the publisher's website.

Acknowledgements This work was funded by the Partner State Key Laboratory on Advanced Displays and Optoelectronics Technologies (PSKL) though project no. ITC-PskL12EG02. We thank Prof. Zhiyong Fan from Department of Electronic and Computer Engineering and Prof. He Yan from Department of Chemistry to provide the help of IPCE measurement. The work was partially supported by a grant from the Research Grants Council of the Hong Kong Special Administrative Region, China, under Theme-based Research Scheme through project no. T23-713/11-1.

References

[1] A. Kojima, K. Teshima, Y. Shirai, and T. Miyasaka, J. Am. Chem. Soc. **131**, 6050 (2009).
[2] W. S. Yang, J. H. Noh, N. J. Jeon, Y. C. Kim, S. Ryu, J. Seo, and S. I. Seok, Science **348**, 1234 (2015).
[3] M. A. Green, K. Emery, Y. Hishikawa, W. Warta, and E. D. Dunlop, Prog. Photovolt.: Res. Appl. **23**, 1 (2015).
[4] G. Xing, N. Mathews, S. Sun, S. S. Lim, Y. M. Lam, M. Gratzel, S. Mhaisalkar, and T. C. Sum, Science **342**, 344 (2013).
[5] H. J. Snaith, J. Phys. Chem. Lett. **4**, 3623 (2013).
[6] S. D. Stranks, G. E. Eperon, G. Grancini, C. Menelaou, M. J. P. Alcocer, T. Leijtens, L. M. Herz, A. Petrozza, and H. J. Snaith, Science **342**, 341 (2013).
[7] G. Li, K. L. Ching, J. Y. L. Ho, M. Wong, and H.-S. Kwok, Adv. Energy Mater. **5**, 1401775 (2015).
[8] M. Liu, M. B. Johnston, and H. J. Snaith, Nature **501**, 395 (2013).
[9] J. Burschka, N. Pellet, S.-J. Moon, R. Humphry-Baker, P. Gao, M. K. Nazeeruddin, and M. Grätzel, Nature **499,** 316 (2013).
[10] Q. Chen, H. Zhou, Z. Hong, S. Luo, H.-S. Duan, H.-H. Wang, Y. Liu, G. Li, and Y. Yang, J. Am. Chem. Soc. **136**, 622 (2014).
[11] P. Luo, Z. Liu, W. Xia, C. Yuan, J. Cheng, and Y. Lu, ACS Appl. Mater. Interf. **7**, 2708 (2015).
[12] Y. Li, J. K. Cooper, R. Buonsanti, C. Giannini, Y. Liu, F. M. Toma, and I. D. Sharp, J. Phys. Chem. Lett. **6**, 493 (2015).
[13] M. R. Leyden, L. K. Ono, S. R. Raga, Y. Kato, S. Wang, and Y. Qi, J. Mater. Chem A **2**, 18742 (2014).
[14] B. S. Tosun and H. W. Hillhouse, J. Phys. Chem. Lett. **6**, 2503 (2015).
[15] P. Luo, Z. Liu, W. Xia, C. Yuan, J. Cheng, and Y. Lu, J. Mater. Chem. A **3**, 12443 (2015).
[16] A. J. Ritenour, J. W. Boucher, R. DeLancey, A. L. Greenaway, S. Aloni, and S. W. Boettcher, Energy Environ. Sci. **8**, 278 (2015).
[17] T. C. Anthony, J. Vac. Sci. Technol. **2**, 1296 (1984).
[18] G. F. Pérez-Sánchez, F. Chávez, D. Cortés-Salinas, P. Zaca-Morán, A. Morales-Acevedo, R. Peña-Sierra, O. Goiz, and A. T. Huerta, Vacuum **107**, 236 (2014).
[19] M. A. Green, K. Emery, Y. Hishikawa, W. Warta, and E. D. Dunlop, Prog. Photovolt.: Res. Appl. **21**, 827 (2013).
[20] J. R. Groza and J. F. Shackelford, Materials Processing Handbook (CRC Press, 2007).
[21] S. Colella, E. Mosconi, P. Fedeli, A. Listorti, F. Gazza, F. Orlandi, P. Ferro, T. Besagni, A. Rizzo, G. Calestani, G. Gigli, F. De Angelis, and R. Mosca, Chem. Mater. **25**, 4613 (2013).
[22] H. Yu, F. Wang, F. Xie, W. Li, J. Chen, and N. Zhao, Adv. Funct. Mater. **24**, 7102 (2014).
[23] W. Zhang, M. Saliba, D. T. Moore, S. K. Pathak, M. T. Hörantner, T. Stergiopoulos, S. D. Stranks, G. E. Eperon, J. A. Alexander-Webber, A. Abate, A. Sadhanala, S. Yao, Y. Chen, R. H. Friend, L. A. Estroff, U. Wiesner, and H. J. Snaith, Nature Commun. **6**, 6142 (2015).
[24] A. Dualeh, P. Gao, S. I. Seok, M. K. Nazeeruddin, and M. Grätzel, Chem. Mater. **26**, 6160 (2014).
[25] P. Löper, M. Stuckelberger, B. Niesen, J. Werner, M. Filipič, S.-J. Moon, J.-H. Yum, M. Topič, S. De Wolf, and C. Ballif, J. Phys. Chem. Lett. **6**, 66 (2015).
[26] J. M. Ball, S. D. Stranks, M. T. Hörantner, S. Hüttner, W. Zhang, E. J. W. Crossland, I. Ramirez, M. Riede, M. B. Johnston, R. H. Friend, and H. J. Snaith, Energy Environ. Sci. **8**, 602 (2015).